Monthly Notices
of the
ROYAL ASTRONOMICAL SOCIETY

Mon. Not. R. Astron. Soc. **419,** 1097–1106 (2012) doi:10.1111/j.1365-2966.2011.19765.x

The EVN Galactic Plane Survey – EGaPS

Leonid Petrov★

ADNET Systems, Inc./NASA GSFC, Code 610.2, Greenbelt, MD 20771, USA

Accepted 2011 September 3. Received 2011 August 30; in original form 2011 June 23

ABSTRACT

I present a catalogue of the positions and correlated flux densities of 109 compact extragalactic radio sources in the Galactic plane determined from an analysis of a 48-h Very Long Baseline Interferometry (VLBI) experiment at 22 GHz with the European VLBI Network. The median position uncertainty is 9 mas. The correlated flux densities of the detected sources are in the range of 20–300 mJy. In addition to the target sources, nine water masers have been detected, of which two are new. I derived the positions of the masers with an accuracy of 30–200 mas and determined the velocities of the maser components and their correlated flux densities. The catalogue and the supporting material are available at http://astrogeo.org/egaps.

Key words: instrumentation: interferometers – catalogues – surveys – astrometry.

1 INTRODUCTION

The differential Very Long Baseline Interferometry (VLBI) astrometry has become a powerful instrument for the study of the 3D structure and dynamics of our Galaxy (see, for instance, Brunthaler et al. 2011). The analysis of differential observations allows us to determine parallaxes of compact radio sources with accuracies down to several tens of microarcseconds, positions with uncertainties of 0.05 mas and proper motions. The differential astrometry observations are made in the so-called phase-referencing mode in which the radio telescopes of a VLBI network rapidly switch from a target source to a nearby calibrator. The analysis of differential fringe phases allows us to dilute the contribution of mismodelled path delays in the atmosphere by a factor of the target-to-calibrator separation in radians, i.e. 20–50 times. Nowadays, observations in the phase-referencing mode are widely used for imaging faint sources. The atmospheric path delay fluctuations limit the integration time, depending on frequency, to 0.2–10 min. Phase referencing observations allow us to overcome this limit and to integrate the signal for hours. According to Wrobel (2009), 63 per cent of Very Long Baseline Array (VLBA) observations in 2003–2008 were made in the phase-referencing mode.

However, the feasibility of phase-referencing observations is determined by the availability of a pool of calibrators with precisely known positions. The first catalogue of source coordinates determined with VLBI contained 35 objects (Cohen & Shaffer 1971). Since then, hundreds of sources have been observed under geodesy and astrometry VLBI observing programmes at 8.6 and 2.3 GHz (*X* and *S* bands) using the Mark3 recording system at the International VLBI Service for Geodesy and Astrometry (IVS) network. Analyses of observations made in 1980s and 1990s led to the compilation of the International Celestial Reference Frame (ICRF) catalogue of 608 sources (Ma et al. 1998). Later, using the VLBA, the positions of over 5000 other compact radio sources were determined in the framework of the VLBA Calibrator Survey (VCS) (Beasley et al. 2002; Fomalont et al. 2003; Petrov et al. 2005, 2006, 2007a; Kovalev et al. 2007), the VLBA Image and Polarization Survey (VIPS) (Helmboldt et al. 2007; Petrov & Taylor 2011e), the BeSSel Calibrator Survey (Immer et al. 2011), and in a number of ongoing programmes: the geodetic VLBA programme RDV (Petrov et al. 2009), the programme of the study of active galaxy nuclei (AGNs) at parsec scales detected with *Fermi* (Kovalev et al., in preparation[1]), the programme of observing radio-loud galaxies from the Two Micron All-Sky Survey (2MASS) (Condon et al., in preparation[2]), and the programme of observing optically bright quasars (Bourda, Charlot & Le Campion 2008; Bourda et al. 2011; Petrov 2011). The use of the Australian Long Baseline Array (LBA) extended the catalogue of calibrators to the zone [− 90°, −40°] (Petrov et al. 2011c).

By 2011 July, the total number of radio sources with positions determined with VLBI in the absolute astrometry mode reached 6455[3] and it continues to grow. *On average*, the probability of finding a calibrator within a 3° radius of a given position is 97 per cent. However, the density of calibrators in the Galactic plane is still low and an increase in the number of calibrators is badly needed for many VLBI Galactic astronomy projects. Finding extragalactic sources visible through the Galactic plane region is more difficult for several reasons. First, the region is crowded with many galactic objects. Combining independent low-resolution observations at different frequencies makes determination of their spectra problematic due to the risk of source misidentification. Secondly, many potential candidates with flat spectra are extended Galactic objects, such as planetary nebulae or compact H II regions, which cannot be detected

[1] See http://astrogeo.org/faps.
[2] See http://astrogeo.org/v2m.
[3] See http://astrogeo.org/rfc for the most recent VLBI position catalogue.

★E-mail: Leonid.Petrov@lpetrov.net

with VLBI. Thirdly, the apparent angular size of extragalactic objects observed through a high plasma density near the Galactic plane is broadened by Galactic scattering and cannot be detected at low frequencies on baselines longer than several thousand kilometres.

To address the problem of increasing the density of calibrators within the Galactic plane, Petrov et al. (2007b) made in 2005–2006 a dedicated blind fringe survey of 2496 objects with the VERA (VLBI Exploration of Radio Astrometry) radio interferometer (Honma, Kawaguchi & Sasao 2000) in *K* band (22 GHz). Those sources which were detected with VERA were re-observed with VLBA in 2006 in *K* band in the framework of the VGaPS campaign (Petrov et al. 2011b). These observations allowed us to determine the positions of 176 new sources within 6° of the Galactic plane with a median accuracy of 0.9 mas. The detection limit of VERA was 200–300 mJy, the detection limit of the follow-up VLBA observations was 70–90 mJy depending on the baseline.[4] Independently, a team led by Mark Reid searched for Galactic plane calibrators in 2010 using VLBA in the framework of the Bar and Spiral Structure Legacy Survey (BeSSeL) project (Brunthaler et al. 2011) and reported detection of 198 sources (Immer et al. 2011), of which 82 were new.

In this paper I present the results of a 48-h experiment at the European VLBI Network (EVN) observed in 2009 October, called the EVN Galactic Plane Survey (EGaPS). The goal of this experiment was to further increase the calibrator source density in the zone within 6° of the Galactic plane and with declinations $>-20°$. Using highly sensitive antennas, sources as weak as 20 mJy were detected, a factor of 4 weaker than in the prior VGaPS campaign. These calibrators are aimed to be used for Galactic astronomy projects. The selection of candidate sources and the scheduling strategy are discussed in Section 2. The station set-up during the observing sessions is described in Section 3. The correlation and post-correlation analyses are discussed in Section 4. The catalogue of source positions and correlated flux densities is presented in Section 6. An error analysis of observations, including the evaluation of systematic errors, is given in Section 4.3, and the results are summarized in Section 7.

2 CANDIDATE SOURCE SELECTION

In the past, the list of bright compact sources detected with the Very Large Array (VLA) and/or Multi-Element Radio Linked Interferometer Network (MERLIN) served as a pool for candidate sources for VLBI calibrator surveys. Almost all these objects have already been observed with VLBA. Since the combined catalogue of sources observed in the absolute astrometry mode is complete at the 150–200 mJy level, new calibrators should be relatively faint objects. Most all-sky surveys at frequencies higher than 2 GHz are either incomplete or not deep enough, or both. As a result, information about spectral indices is sparse and often unreliable. For this reason, it is rather difficult to find the remaining good flat spectrum candidate sources.

New calibrator candidates were found by analysing 395 radio astronomical catalogues using the Catalogue support System (CATS) data base (Verkhodanov et al. 1997). The data base includes the NRAO VLA Sky Survey (NVSS) (Condon et al. 1998), the Cosmic Lens All-Sky Survey (CLASS) (Myers et al. 2003), the Combined Radio All-Sky Targeted Eight GHz Survey (CRATES) (Healey et al. 2007), the Australia Telescope Compact Array (ATCA) survey at 20 GHz (AT20G) (Murphy et al. 2010), and many other catalogues. Initially, I selected 1100 sources that satisfy the following criteria:

(i) were not observed previously with VLBI;
(ii) have Galactic latitude $|b| < 6°$;
(iii) have declination $>-20°$;
(iv) have at least two measurements of their flux density that allow the estimation of their spectral indices at frequencies higher than 2 GHz;
(v) have single-dish flux densities extrapolated to 22 GHz $>$ 80 mJy;
(vi) have spectral indices α flatter than -0.5 ($S \sim \nu^{\alpha}$).

The majority of these sources were selected by cross-identification of the NVSS and GB6 (Gregory et al. 1996) catalogues. Then I scrutinized the source spectra and rejected approximately 50 per cent of the sources with unreliable spectra or the objects known as Galactic sources. The remaining list contains 559 candidates.

Figure 1. The EVN stations that participated in the EGaPS experiment. The longest meridional baselines NOTO/ONSALA60 is 2280-km long. The longest longitudinal baseline NOTO/YEBES40M is 1616-km long.

2.1 Observation scheduling

The following stations were scheduled for 48-h observations: EFLSBERG, JODRELL2, MEDICINA, NOTO, ONSALA60, and YEBES40M (see Fig. 1 and Table 1). The observation schedule was prepared with the dedicated software program SUR_SKED.[5] The scheduling goal was to observe each target source at all antennas of the array in two scans of 120 s each.

The scheduling algorithm implemented in SUR_SKED found the sequence of sources that minimized the slewing time. The minimum

[4] The *K*-band receivers at the VLBA stations were upgraded in 2007 after these observations, which improved the sensitivity of the array at 24 GHz at the same recording rate by a factor of 2 according to Walker et al. (2008).

[5] See http://astrogeo.org/sur_sked for more information.

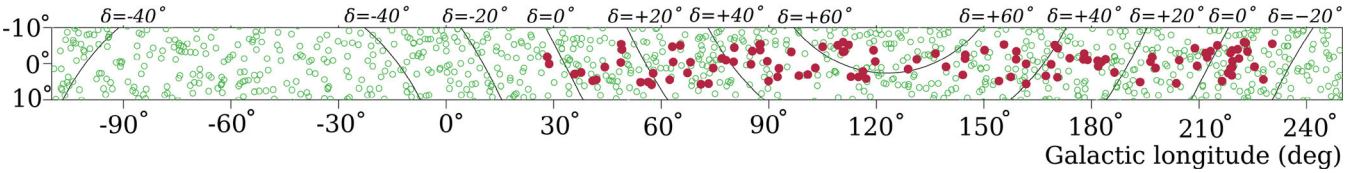

Figure 2. The distribution of calibrator sources within 10° of the Galactic plane. The filled discs denote sources detected in the EGaPS campaign. The hollow circles denote calibrator sources known from previous observations. New sources from the BeSSeL Calibrator Survey are not shown.

Table 1. The EVN stations participated in the EGaPS experiment. The first column shows the IVS station code. The second and third columns show the location of the closest city and the antenna diameter. The average system equivalent flux density (SEFD) achieved in the EGaPS experiment is shown in column 4. The last two columns show the station geocentric latitude and longitude.

IVS code	Location	Diam (m)	SEFD (Jy)	$\phi_{\rm geoc}$	λ
EFLSBERG	Bonn, Germany	100	190	50.°33	6.°88
JODRELL2	Jodrell Bank, UK	25	6840	53.°05	−2.°31
MEDICINA	Bologna, Italy	32	1480	44.°33	11.°65
NOTO	Noto, Italy	32	1884	36.°69	14.°99
ONSALA60	Göteborg, Sweden	18	2790	57.°22	11.°92
YEBES40M	Guadalajara, Spain	40	770	40.°33	−3.°09

time between consecutive observations of the same source was set to 4 h. For deciding which source to put into the schedule, the algorithm calculated the elevation of each candidate object, the slewing time, the time interval between the previous observation of the same source, and the ratio of the remaining visibility time to the total visibility time. For each source with the elevation exceeding 15° above the horizon at every station of the array, a score was computed. The score is a function of the slewing time, the ratio of the remaining visibility time to the total visibility time, and the time interval from the previous observation. A source with the highest score was put into the schedule and then the procedure was repeated.

Every 1.5 h a burst of four strong compact sources with known maps from the *K*/*Q* survey (Lanyi et al. 2010) was observed: two strong objects at the elevation angles of 10°–30° and two strong objects at the elevations of 50°–90°. The purpose of scheduling these calibrators was (a) to allow the estimation of the troposphere path delay in zenith direction; (b) to evaluate the atmosphere opacity; (c) to use them for complex bandpass calibration; (d) to provide a strong connection between the new catalogue and the old catalogue of compact sources.

The schedule had 369 target objects and 69 calibrators. Among the target sources, 344 objects were observed in two scans and 25 sources were observed in one scan. The distribution of known calibrator sources within 10° of the Galactic plane is shown in Fig. 2.

3 OBSERVATIONS

Observations took place on 2009 October 27–29. Eight intermediate frequencies (IFs), both upper and lower sub-band in the range of [22.09999, 22.35599] GHz were observed in a single left circular polarization. The data were recorded with the Mark-5 system, with 2-bit sampling and an aggregate rate of 1024 Mb s^{-1}. The contiguous frequency set-up is far from optimal for an absolute astrometry experiment that utilizes group delays, since the uncertainties of a group delay at a given signal-to-noise ratio is reciprocal to the root mean squares of intermediate frequencies over the band. Two stations, MEDICINA and ONSALA60, could record within 720 MHz, three stations equipped with the VLBA data acquisition system, EFLSBERG, NOTO, and YEBES40M, could record within 500 MHz, and JODRELL2 could record only within 160 MHz. Spreading IFs over 500 MHz would reduce the group delay uncertainty by a factor of 2.4 at all baselines, except for JODRELL2 where it would increase the uncertainty by a factor of 2 since some channels will be missing. However, in order to record a band wider than 256 MHz, the local oscillator (LO) frequency should be changed with respect to those that are used in other EVN experiments. This would require manual intervention. When I realized that for logistical reasons there is a high risk that it may not be possible to make this change at some stations, which could ruin the experiment, I fell back on the contiguous frequency set-up.

The station YEBES40M lost the first 7 h of the experiment because of the Mark-5B failure. The system temperature of YEBES40M was around 210 K during the next 3 h because the vertex was closed. It dropped to the normal range of 60–100 K when the operator noticed it and opened the vertex. The station JODRELL2 did not show fringes in IF11–IF16.

4 DATA ANALYSIS

The analysis of the EGaPS data is similar to that performed for the VLBA Galactic Plane Survey. A detailed description of the analysis technique can be found in Petrov et al. (2011b). Here the analysis procedure is briefly outlined.

4.1 Data correlation and post-correlation analysis

The data were correlated at the Bonn DiFX software correlator (Deller et al. 2007) with an accumulation period of 0.12 s and with a spectral resolution of 125 kHz. These correlation parameters provided a field of view over 1 arcmin, comparable to the width of the beam of the EFLSBERG radio telescope. I anticipated that the a priori source coordinates of some of the sources may be wrong at the arcminute level due to source misidentification.

The correlator generates the spectrum of the cross-correlation function that was written in the format compliant with the FITS-IDI specifications (Greisen 2009). Data analysis was performed with the software PIMA.[6] At the first step, the fringe amplitudes were corrected for signal distortion in the sampler. Observations of strong sources were used for deriving complex bandpasses. Since in 2010 the DiFX correlator did not have the ability to extract phase calibration signals from the data, no phase calibration was applied. After that, the group delay, phase delay rate, group delay rate, and fringe phase were determined for each scan at each baseline using the fringe-fitting procedure. These estimates maximize the sum of the

[6] Available at http://astrogeo.org/pima.

cross-correlation spectrum coherently averaged over all the accumulation periods of a scan and over all the frequency channels in all the IFs. A set of estimates of group and phase delays and their first derivatives for a given scan at a given baseline is thereafter called observation. After the first run of fringe fitting, eight observations at each baseline with the strongest signal-to-noise ratio were used to adjust the station-based complex bandpass corrections, and the procedure of computing group delays was repeated with the bandpass applied.

Then the results of fringe fitting were exported to the VTD/post-Solve VLBI analysis software[7] for interactive processing group delays of those observations which had the signal-to-noise ratio high enough to ensure that the probability of false detection be less than 0.001. An analysis of the probability distribution function of the achieved signal-to-noise ratios allowed me to find that the probability of a false detection in this experiment is less than 0.001 when signal-to-noise ratio >6.14. The theoretical path delays were computed according to the state-of-the-art parametric model, as well as their partial derivatives. The model included the contribution of the ionosphere to group delay and phase delay rates computed using the total electron content maps derived from the analysis of Global Positioning System (GPS) observations by the analysis centre CODE (Schaer 1998). Small differences between group delays and theoretical path delays as well as between the measured and theoretical delay rates were used for an interactive estimation of corrections to a parametric model that describes the observations with least squares (LSQ). The coordinates of the target sources, the positions of all the stations except the reference one, the parameters of the splines that describe corrections to the a priori path delay in the neutral atmosphere in the zenith direction for all the stations, and the parameters of other splines that describe the clock function, were solved in a single LSQ solution using group delays. Outliers were identified and temporarily suppressed, and additive corrections to weights of observables were determined. Then the fringe-fitting procedure was repeated for outliers with phase delay rates and group delays evaluated in a narrow window around the expected value computed on the basis of results of the previous LSQ solution. New estimates of group delays for points with probabilities of false detection less than 0.1, which corresponds to a signal-to-noise ratio >4.9 for the narrow fringe search window, were used in the next step of the interactive analysis procedure. For observations made with the narrow window search, the outlier status was lifted. Parameter estimation, elimination of the remaining outliers and adjustments of additive weight corrections were then repeated. In total, group delays of 2471 observations out of the 116 75 scheduled were used for further processing. There were 178 sources detected in 3–66 observations, including 109 target sources and 69 calibrators. Sources that had only one or two used observations were discarded from further analysis since the condition of providing a minimum redundancy for the quality control of position estimates was not met.

4.2 Source position determination

The results of the interactive solution provided a clean data set of group delays with updated weights from the EGaPS experiment. The data set that was used for the final parameter estimation utilized all of the dual-band *S/X* data acquired under absolute astrometry and space geodesy programmes from 1980 April through 2011 February and included the *K*-band data from the EGaPS experiment, in total 8 million observations. The estimated parameters are right ascensions and declinations of all the sources, coordinates and velocities of all the stations, coefficients of B-spline expansion of the non-linear motion for 16 stations, coefficients of harmonic site position variations of 48 stations at four frequencies – annual, semi-annual, diurnal and semidiurnal – and axis offsets for 67 stations. They were adjusted using all of the data. The estimated parameters also included the Earth orientation parameters for each observing session, parameters of clock function and residual atmosphere path delays in the zenith direction modelled with the linear B-spline with the intervals of 60 and 20 min, respectively. All the parameters were estimated in a single LSQ run.

The system of LSQ equations has an incomplete rank and defines a family of solutions. In order to pick a specific element from this family, I applied the no-net-rotation constraints on the positions of 212 sources marked as 'defining' in the ICRF catalogue (Ma et al. 1998) which required the positions of these sources in the new catalogue to have no rotation with respect to the position in the ICRF catalogue. The no-net-rotation and no-net-translation constraints on the positions and linear velocities of 48 stations with respect to the values listed in the ITRF2000 catalogue (Altamimi, Sillard & Boucher 2002) were also applied. These stations participated in at least 50 VLBI experiments for at least 3 years. This specific choice in identifying the constraints was made so as to preserve the continuity of both the new catalogue source coordinates and the station positions with the other VLBI solutions obtained during the last 15 years.

The global solution sets the orientation of the array with respect to the ensemble of >5000 extragalactic remote radio sources. The orientation is defined by the continuous series of the Earth orientation parameters and parameters of the empirical model of site position variations over 30 years evaluated together with source coordinates. The common sources observed in the EGaPS experiment as amplitude calibrators provided a connection between the new catalogue and the old catalogue of compact sources.

A valuable by-product of the analysis of the EGaPS observations is the estimates of the JODRELL2 positions (see Table 2). This is the second experiment with the participation of this station under astrometry or geodesy programmes. The previous EVN experiment, TP001, carried out on 2000 November 23, was made at 5 GHz with a bandwidth spread of over 108 MHz (Charlot et al. 2002). A comparison of the results of a re-analysis of TP001 and EGaPS made using exactly the same a priori model and parameter estimation technique showed that the differences between the JODRELL2 positions reduced to the J2000.0 epoch using the velocities predicted by the NNR-NUVEL1A plate tectonic model (DeMets et al. 1994) are 38, 20 and 9 mm at *X*, *Y* and *Z* coordinates, respectively. Although the position of JODRELL2 from the 5-GHz observations with formal uncertainties of 10–20 mm suffered from residual errors in modelling path delay through the ionosphere which are

Table 2. Estimates of the JODRELL2 positions in metres in the crust fixed geocentric coordinate system on epoch 2009.10.27.

X	$3822\,846.633 \pm 0.026$
Y	$-153\,802.071 \pm 0.009$
Z	$5086\,286.064 \pm 0.036$

[7] Available at http://astrogeo.org/vtd.

20 times greater than those at 22 GHz, the differences in positions are within 1–2 reported uncertainties.

4.3 Position error analysis

The formal uncertainties of the semimajor axes of the error ellipses of the position estimates of the 109 target sources range from 2 to 60 mas with a median value of 8 mas. They are based on the error propagation law of group delay uncertainties derived by the fringe-fitting procedure.

Including in the observing schedule a considerable number of calibrator sources with positions known at the sub-mas level facilitated the error analysis. In order to evaluate the level of systematic errors, I used a similar technique that was developed for processing the VGaPS observations. The list of 69 calibrators was ordered by the increase in their right ascensions and split into two subsets with even and odd indices. I made two special global solutions using all the data from 1980 through 2011. In solution A, calibrators with even indices were excluded from all the experiments but EGaPS. In solution B, calibrators with odd indices were excluded from all the experiments but EGaPS. I compared the positions of the calibrator sources from solutions A and B with their positions from the dual-band global solution C that used all the sources in all the experiments except EGaPS. The positions of the sources from solution C were determined with accuracies of 0.1–0.3 mas, which can be considered true for the purpose of this comparison.

The weighted root mean square (wrms) of the differences of 69 calibrator sources from special solutions A and B and the reference solution C are 1.8 mas in declinations and 3.7 mas in right ascensions scaled by $\cos\delta$ with χ^2 per degree of freedom 1.3 and 3.3, respectively. If added in quadrature to uncertainties in right ascensions and declinations, the noise with the standard deviations being 4.0 mas/$\cos\delta$ and 1.0 mas, respectively, the χ^2 per degree becomes close to 1. Therefore, I inflated the reported uncertainties in right ascensions and declinations of target sources by 4.0 mas/$\cos\delta$ and 1.0 mas, respectively, in quadrature.

4.4 Data analysis: correlated flux density determination

Each detected target source has 3–28 observations with the median number being eight. The data set is too sparse to produce meaningful images. In this study I limited my analysis with mean correlated flux density estimates to two ranges of lengths of the baseline projections on to the plane tangential to the source without inversion of the calibrated visibility data. The information about the correlated flux density is needed for evaluation of the required integration time when an object is used as a phase calibrator.

An analysis of the system temperature measurements revealed variations both with time and with elevation angle. The measured system temperature is considered as a sum of two terms: the receiver temperature $T_{\rm r}$ and the contribution of the atmosphere:

$$T_{\rm sys} = T_{\rm r} + T_{\rm atm}[1 - {\rm e}^{-\beta\, m(e)}], \tag{1}$$

where $T_{\rm atm}$ is the average temperature of the atmosphere, β is the atmosphere opacity and $m(e)$ is the wet mapping function: the ratio of the non-hydrostatic constituent of the path delay in the neutral atmosphere at the elevation e to that path delay in the zenith direction. I omitted in expression (1) the ground spill-over term that was not determined for these antennas. Both the receiver temperature and the atmosphere opacity depend on time. Since in the astrometric analysis I estimated for each station the non-hydrostatic component of the atmosphere path delay in the zenith direction which is closely related to the integrated column of the water vapour, I was able to use these estimates for modelling the time dependence of the opacity. I present the system temperature as

$$T_{\rm sys} = \sum_i T_{{\rm r}i}\, B_i^1(t) + T_{\rm atm}[1 - {\rm e}^{-(a+b\tau_{\rm atm}(t))m(e)}], \tag{2}$$

where a and b are empirical coefficients that relate the opacity and the estimates of the atmosphere path delay, $\tau_{\rm atm}(t)$ is the estimate of the non-hydrostatic atmosphere path delay, $B_i^1(t)$ is the B-spline of the first degree with the pivotal element i, and $T_{{\rm r}i}$ are the coefficients of the expansion of the receiver temperature into the B-spline basis. I set $T_{\rm atm}$ to 280 K, and evaluated the coefficients of the receiver temperature and regression parameters a and b by fitting them into the measurements of the system temperatures using the non-linear LSQ. Parameter a describes a possible bias between estimates of the integrated water vapour contents and the non-hydrostatic path delay in the zenith direction. The system temperature divided by ${\rm e}^{-[a+b\tau_{\rm atm}(t)]\,m(e)}$ is free from absorption in the atmosphere and is equivalent to that at the top of the atmosphere.

The rms values of the residuals of the empirical model of the system temperature are in the range of 2–8 K. The time variations of $T_{\rm r}$ were within 10 K at EFLSBERG, JODRELL2, MEDICINA and NOTO. The $T_{\rm r}$ was around 180 K during the first 3 h at YEBES40M and then suddenly dropped to 30 K when the operator opened the vertex, and after that stayed stable. The $T_{\rm r}$ at ONSALA60 was unstable during the entire experiment and varied in the range of 40–250 K.

The fringe amplitudes were calibrated by multiplying them by the system temperature reduced to the top of the atmosphere and dividing by the elevation-dependent a priori gain.

The a priori antenna gain and/or the term $T_{\rm sys}/{\rm e}^{[-a+b\tau_{\rm atm}(t)]\,m(e)}$ may have a multiplicative error. The corrections to the antenna gain were evaluated by fitting the correlated amplitude to the flux density of sources with known brightness distributions. Among the sources used as amplitude calibrators, brightness distributions are publicly available[8] for 45 objects from the *K*/*Q* survey and the VGaPS observing campaigns.

For each observation of an amplitude calibrator with a known brightness distribution in the form of CLEAN components, I predicted the correlated flux density F to be

$$F_{\rm corr} = \left| \sum_i c_i\, {\rm e}^{\frac{2\pi f}{c}(u\,x + v\,y)} \right|, \tag{3}$$

where c_i is the correlated flux density of the ith CLEAN component with the coordinates x and y with respect to the centre of the image, and u and v are the projections of the baseline vectors on the tangential plane of the source.

Then I built a system of least-squares equations for all the observations of calibrators with known brightness distributions used in the astrometric solution:

$$F_{\rm corr} = \sqrt{g_i\, g_j}\, A_{\rm corr}, \tag{4}$$

and after taking logarithms from left- and right-hand sides solved for time-independent corrections to gains g_i for all the stations using LSQ. Finally, I applied corrections to gains for observations of all other sources.

[8] The data base of brightness distributions, correlated flux densities, and images of compact radio sources produced with VLBI is accessible from http://astrogeo.org/vlbi_images.

The gain correction was in the range of 0.7–1.3 for all the antennas, except for JODRELL2. The correction to the JODRELL2 gain was 6.9, and its system equivalent flux density (SEFD) at elevations higher than 50° was around 7000 K.

The detection limit varied significantly between the baselines. Sources as weak as 13–16 mJy had the signal-to-noise ratio >6.14 and therefore, were detected at the most sensitive baseline, EFLSBERG/YEBES40M. The detection limit at the baselines EFLSBERG/MEDICINA and EFLSBERG/NOTO was in the range of 25–30 mJy, at the baseline EFLSBERG/ONSALA60 it was 30–40 mJy, and at the baselines EFLSBERG/JODRELL2 and MEDICINA/NOTO it was 60–70 mJy.

5 DATA ANALYSIS: H_2O MASER SOURCES

When scrutinizing the cross-correlation spectra, I found several objects with very strong peaks in IF9; for example, the object 0221+618 at the baseline MEDICINA/ONSALA60 (see Fig. 3).

This feature of the fringe spectrum is interpreted as an emission from a water maser. The peak frequency of the cross-spectrum is shifted within several megahertz due to a relative motion of the maser with respect to the geocentre. Although this project did not target maser investigation, nevertheless, I decided to systematically search for masers in the data, determine their coordinates and determine the parameters of their spectra.

Processing the data from narrow-band sources differs significantly from processing the data from continuum sources. I searched for masers by running 31 trial fringe-fitting with a spectral window of 1 MHz within IF9 in the range of 22.227 99–22.243 99 GHz. Other spectral constituents were masked out. The spectral window was increased by 0.5 MHz after each run. Since the maser has emission only within a narrow band, suppressing the spectrum beyond the search window improved the signal-to-noise ratio considerably since the amount of noise was reduced, though the power of the signal remained the same. I searched for objects with the peak fringe amplitude being higher than four times the spectrum rms. This approach helped me to discover nine maser objects. After a signal from the masers was detected at least at one baseline, the spectrum filter was narrowed down even further to reduce the contribution of the noise away from the spectral lines. This allowed me to increase the number of detections at the other baselines.

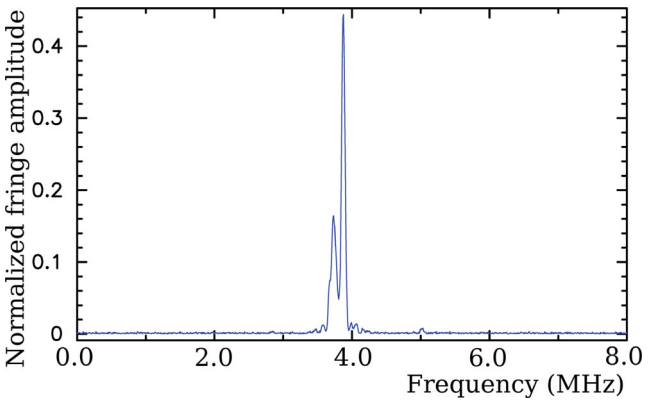

Figure 3. The normalized fringe amplitude of the water maser 0221+618 at baseline MEDICINA/ONSALA60. The horizontal axis shows the frequency offset with respect to the nominal H_2O maser frequency (6_{16}–5_{23}) 22.235 044 GHz.

The frequency resolution of the cross-spectrum, 125 kHz, which corresponds to the Doppler velocity resolution of 1.7 km s^{-1}, is not sufficient to resolve the water maser spectral line. The scans with seven out of nine detected masers were recorrelated with a 16 times higher spectral resolution of 7.8 kHz, which corresponds to the Doppler velocity resolution of 0.1 km s^{-1}. Two other masers, 2130 + 556 and 2247 + 596, were discovered after the media with recorded data was recycled, but it was too late to recorrelate the data.

I smoothed the cross-spectrum and fitted a preliminary model of the amplitude spectrum as a function of frequency f of maser emission $A(f) = \sum_i A_i \exp -\{(f - f_i)^2/s_i^2\}$ using an iterative nonlinear LSQ procedure. Here A_i is the peak amplitude of the component, f_i is its frequency, and s_i is the parameter of the linewidth. After determining a satisfactory preliminary model of the smoothed spectrum, I fitted the final model using the raw cross-spectrum. Since masers are not point-like objects, but usually conglomerates of tens or even hundreds of spots, the correlated flux density at different parts of the *uv*-plane differs considerably due to beatings from different components. Using only 10–20 points at the *uv*-plane is not sufficient for an image reconstruction. Therefore, I restricted the amplitude analysis to the determination of the minimum and maximum correlated flux densities of the detected components at different baselines.

The fringe-fitting process cannot provide a meaningful estimate of a group delay for a narrow-band source. Therefore, I resorted to using phase delay rates for determining the source positions. A phase delay rate of over 2 min of integration time at 1024 Mbps recording rate has the uncertainty due to the thermal noise of the order of 2×10^{-13} per signal-to-noise ratio. However, unmodelled short-term atmosphere path delay fluctuations limit the accuracy of modelling the phase delay rate usually to a level of $0.5–1.0 \times 10^{-13}$. The uncertainty of the phase delay rate equivalent to group delay, σ_r/Ω_n (where Ω_n is the nominal Earth rotation rate) at signal-to-noise ratio = 10 is 300 ps if we take into account only the thermal noise, and 1400 ps if we consider the contribution of the atmosphere path delay rate. The uncertainty of group delay at signal-to-noise ratio = 10 in our experiment is around 200 ps, i.e. a factor of 7 better. If we use only the phase delay rates, the adjustments to nuisance parameters, such as the atmosphere path delays in the zenith direction, station positions and clock functions, will be determined less precisely than from the group delay solution and they will affect the estimates of source coordinates. In order to alleviate the effect of poorly determined nuisance parameters on the estimates of maser positions, I ran a special solution with observation equations using both group delays and phase delay rates for all the detected sources, continuum spectrum objects and masers. The phase delay rates had zero weight for continuum sources and group delays had zero weight for maser sources.

The positions of the maser sources and their uncertainties are presented in Table 3. This table also contains the peak minimum and maximum correlated flux densities for each component of a maser source over observations at different baselines and the velocity with respect to the local system of rest (LSR) assuming that the barycentre of the Solar system is moving at a speed of 20 km^{-1} s in the direction of right ascension $18^h\,03^m\,50\overset{s}{.}24$ and declination $+30°\,00'\,16\overset{''}{.}8$. The table contains the full width at half-maximum (FWHM) of the line profile and the minimum and maximum correlated flux densities integrated over the line profile: $\int F(v)\,dv$. For two sources that were correlated only with the low spectral resolution, the lower limits of their peak correlated flux densities and the lower limits of the FWHM of their line profiles are presented.

Table 3. Properties of detected H_2O masers. Column description: (1) IAU name; (2) common name; (3) *IRAS* designator; (4) right ascension; (5) uncertainty in right ascension in arcsec (without $\cos\delta$ factor); (6) declination; (7) uncertainty in declination in arcsec; (8) component index; (9) minimum correlated flux density in Jy; (10) maximum correlated flux density in Jy; (11) LSR velocity in km^{-1} s; (12) FWHM of the line profile in km^{-1} s; (13) minimum integrated flux density in Jy km^{-1} s; (14) maximum integrated flux density in Jy km^{-1} s.

IVS name (1)	Alt name (2)	*IRAS* name (3)	Right ascension (4)	σ_α (5)	Declination (6)	σ_δ (7)	CI (8)	F_{min} (9)	F_{max} (10)	V_{LSR} (11)	FWHM (12)	I_{min} (13)	I_{max} (14)
0221+618	W3(2)	02219+6152	02 25 40.672	0.13	+62 05 54.06	0.08	1	24.6	52.1	−59.0	0.4	5.7	12.1
							2	6.0	28.3	−58.5	0.3	1.1	5.9
							3	13.7	1039.1	−55.9	0.4	3.3	275.5
							4	4.4	393.4	−54.3	0.6	0.8	120.3
							5	5.6	324.0	−53.6	0.5	0.9	87.7
							6	15.8	346.7	−52.3	0.5	4.5	102.5
							7	12.1	85.7	−51.0	0.4	2.5	26.1
							8	7.4	42.6	−49.7	0.4	1.5	11.4
1907+082		19074+0814	19 09 49.847	0.03	+08 19 45.28	0.20	1	7.5	19.4	104.6	0.5	2.1	5.0
							2	1.8	1.8	112.0	0.4	0.4	0.4
1920+143	W51 W	19209+1421	19 23 11.224	0.03	+14 26 45.80	0.11	1	6.9	9.0	96.5	0.6	1.8	3.8
							2	2.8	26.5	98.6	0.5	0.7	7.4
							3	3.1	9.9	100.1	0.5	0.7	3.8
							4	8.8	34.2	101.9	0.5	2.7	10.2
							5	1.9	5.1	103.3	0.4	0.4	1.4
1923+151		19230+1506	19 25 17.907	0.06	+15 12 24.46	0.17	1	1.6	1.8	53.0	0.5	0.4	0.5
							2	5.3	5.3	55.0	0.8	2.4	2.4
							3	1.7	4.1	57.4	0.4	0.5	0.8
							4	2.6	3.6	58.8	0.4	0.6	0.8
2011+360		20116+3605	20 13 34.296	0.06	+36 14 54.36	0.06	1	8.9	45.4	−19.1	0.3	1.6	7.9
2107+521	WB43	X2107+521	21 09 21.717	0.04	+52 22 37.05	0.03	1	1.5	55.6	−3.5	0.4	0.3	16.0
							2	2.2	41.0	2.4	0.4	0.5	16.6
							3	2.5	63.4	4.1	0.6	0.7	26.1
							4	6.5	17.3	8.7	0.4	1.3	3.8
							5	5.3	25.1	11.8	0.4	1.1	6.5
							6	2.3	40.1	12.8	0.4	0.6	7.5
							7	1.6	37.0	13.8	0.3	0.3	7.7
							8	1.3	38.1	14.8	0.3	0.3	7.5
							9	2.3	99.9	16.2	0.3	0.4	20.3
							10	2.8	16.1	17.4	0.3	0.6	2.8
2130+556		21306+5540	21 32 12.444	0.07	+55 53 49.64	0.04	1	0.8	>32.3	−60.9	<1.7	0.6	25.3
2247+596	S146	X2247+596	22 49 31.474	0.06	+59 55 41.91	0.03	1	1.1	>17.2	−47.4	<1.7	0.8	11.6
2254+617	Cep A	22543+6145	22 56 17.988	0.06	+62 01 49.40	0.04	1	2.7	34.8	−34.2	0.4	0.5	7.7
							2	3.2	31.4	−22.6	0.5	0.6	10.7
							3	2.9	37.4	−16.0	0.6	0.5	15.6
							4	11.7	20.6	−14.7	0.4	2.3	4.3
							5	4.5	5.2	−9.9	0.3	0.9	0.9
							6	21.7	40.1	−7.2	0.4	5.0	11.8
							7	5.7	111.8	−5.9	0.5	1.3	47.9
							8	3.1	217.7	−4.4	0.3	0.6	36.8
							9	5.0	8.4	−2.9	0.5	1.3	1.9
							10	4.9	5.4	0.1	0.3	1.0	1.1
							11	4.3	7.5	1.8	0.5	0.8	2.8

5.1 Comments on individual masers

Cep A. Curiel et al. (2002) reported the detection of a 2-mJy continuum source at 7 mm in the Cep A complex from VLA observations in 1996. The position of that source, which they labelled VLA-mm, is $22^h\,56^m\,17^s.985$ $+62^\circ\,01'\,49''.45$ with an uncertainty of 0.02 arcsec. Our position of Cep A water maser coincides within 1σ with the position of VLA-mm source. Moscadelli et al. (2009) determined the position of the methanol maser associated with this object using phase-referencing VLBI: $22^h\,56^m\,18^s.0970$ and $62^\circ\,01'\,49''.399$ with a submilliarcsecond accuracy. Their position of the methanol maser is within 0.78 arcsec of the water maser.

1923+151 is a new discovery. Its spectrum is shown in Fig. 4. It is associated with IRAS19230+1506 (3.8 arcsec away) and WISE J192517.93+151225.0 (0.8 arcsec away), within 1σ–2σ of the position uncertainty of these catalogues.

2011+360 is a new discovery. Its spectrum is shown in Fig. 5. It is associated with IRAS20116+3605 (8.6 arcsec away). The object was selected by Sunada et al. (2007) as a water maser candidate; observed, but not detected.

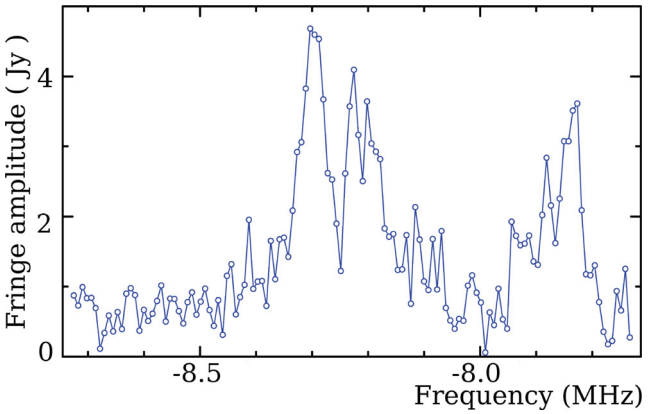

Figure 4. The fringe amplitude of the new water maser 1923+151 at the baseline EFLSBERG/MEDICINA. The horizontal axis shows the frequency offset with respect to the nominal H_2O maser frequency 22.235 044 GHz.

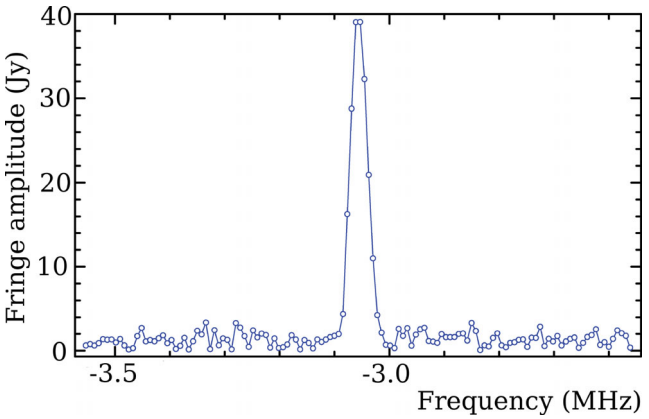

Figure 5. The fringe amplitude of the new water maser 2011+360 at the baseline EFLSBERG/JODRELL2. The horizontal axis shows the frequency offset with respect to the nominal H_2O maser frequency 22.235 044 GHz.

6 THE EGAPS CATALOGUE

Table 4 displays 12 out of the 109 rows of the EGaPS catalogue of source positions. The full table is available as Supporting Information with the electronic version of the article. Columns 2 and 3 contain the J2000 and B1950 IAU names; columns 3 and 4 contain the right ascensions and declinations of the sources. Columns 5 and 6 contain the position errors in right ascension (without multiplier

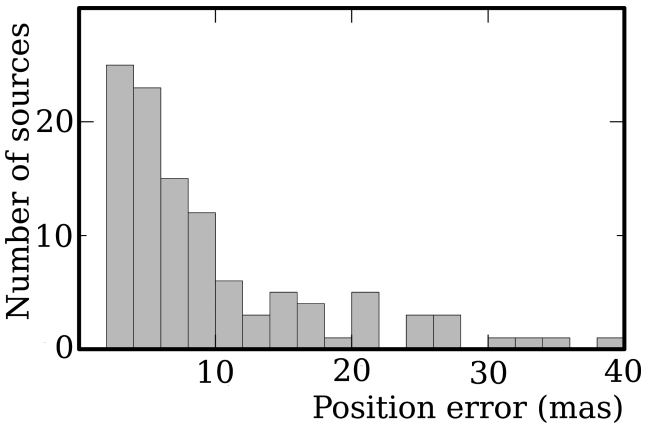

Figure 6. Histogram of the distribution of the semimajor axes of the position uncertainties of 109 objects from the EGaPS catalogue.

cos δ) with noise 4.0 mas/cos δ and 1.0 mas added in quadrature to the formal position uncertainties in right ascension and declination, respectively. Column 7 contains correlation coefficients between right ascension and declination, column 8 contains the total number of observations used in the position data analysis. Columns 9 and 10 contain the median estimates of the correlated flux density over all the experiments of the source in two ranges of baseline projection lengths: 0–67 $M\lambda$ (projections shorter than 900 km) and 100–170 megawavelengths ($M\lambda$) – projections longer than 1350 km. If there were no scheduled observations or no detections at a given range of the baseline projection lengths, then −1.000 is given in the table cell.

The semimajor axes of the position errors range from 4 to 60 mas, and the median position uncertainty is 9 mas. The histogram of the distribution of the final semimajor axes of the position uncertainties is given in Fig. 6. The median uncertainty in right ascension with the cos δ factor is 8.7 mas, while the median uncertainty in declination is 5.9 mas, 1.5 times less. This disparity is due to the elongation of the network in the latitudinal direction: the ratio of the longest polar baseline projection to the longest equatorial baseline projection is 1.4 (see Fig. 1). If the station ONSALA60 or YEBES40M, or both, are dropped for a given source because of non-detections, the disparity further increases.

The uncertainties of the medians of the correlated flux densities are considered to be around 20 per cent. This estimate was made on the basis of (1) applying this method of evaluation of the correlated

Table 4. The first 12 rows of the EGaPS catalogue of the source positions of 109 target sources. The table columns are explained in the text. The full table is available as Supporting Information with the electronic version of the article.

IVS name	IAU name	Right ascension (h min s)	Declination (° ′ ″)	$\Delta\alpha$ (mas)	$\Delta\delta$ (mas)	Corr	# Obs	Flux (Total) (Jy)	Flux (Unres) (Jy)
(1)	(2)	(3)	(4)	(5)	(6)	(7)	(8)	(9)	(10)
0002+576	J0004+5754	00 04 50.263 646	+57 54 57.759 26	15.95	18.90	−0.159	4	0.022	−1.000
0008+657	J0011+6603	00 11 38.823 302	+66 03 38.514 26	26.07	5.01	0.245	7	0.043	−1.000
0017+627	J0019+6300	00 19 47.644 959	+63 00 46.633 73	28.08	4.99	0.094	8	0.037	0.047
0133+602	J0136+6032	01 36 56.806 879	+60 32 05.069 34	23.94	6.31	−0.159	7	0.035	−1.000
0158+623	J0201+6237	02 01 52.980 387	+62 37 57.122 79	47.95	11.05	−0.305	4	0.025	−1.000
0245+620	J0248+6214	02 48 58.890 890	+62 14 09.662 82	18.75	5.91	−0.296	6	0.057	−1.000
0252+574	J0256+5736	02 56 29.004 510	+57 36 42.456 01	11.63	4.59	−0.013	9	0.070	−1.000
0313+531	J0317+5318	03 17 01.346 538	+53 18 27.519 02	19.11	9.83	0.225	4	0.032	−1.000
0334+565	J0338+5640	03 38 36.909 254	+56 40 50.053 81	10.61	3.26	0.034	11	0.071	0.078
0339+573	J0343+5729	03 43 44.815 127	+57 29 08.527 64	25.37	8.68	0.174	5	0.034	−1.000
0357+457	J0400+4554	04 00 34.574 245	+45 54 24.055 05	10.28	5.49	0.204	7	0.068	−1.000

flux density to the *K*-band observations of the VLBA Galactic plane Survey (Petrov et al. 2011b) and comparing the medians of the correlated flux densities derived by this method with those computed from the brightness distributions produced by the self-calibration analysis procedure; and (2) computing the rms of the scatter of the ratios of the correlated flux densities of all the EGaPS sources which have three or more observations. The major contributor to the error budget is the variability of the calibrator sources. Even though the brightness of some individual sources may change significantly, the average correlated flux density of the 69 sources is rather stable. A detailed description of the method for an evaluation of the correlated flux density uncertainties can be found in Petrov, Honma & Shibata (2011a).

7 SUMMARY

I determined the positions of 109 compact extragalactic sources that are within 6° of the Galactic plane with declinations $>-20°$. Observations were made at a six-element array of EVN at 22 GHz. As a result of these observations, the total number of calibrator sources with precisely known positions in this region grew from 322 to 431.

Among the sources detected, nine water masers in our Galaxy were identified of which two are new. The data from seven of these objects were recorrelated with a spectral resolution of 0.1 km s^{-1}. I determined the position of masers from delay rates with accuracies of 30–200 mas and determined the velocities of the components and their correlated flux densities.

I also obtained the estimates of the correlated flux densities of the target extragalactic sources. They are in the range of 20–300 mJy with a median value of 55 mJy.

The results of this campaign are somewhat disappointing. The median position accuracy is 1 order of magnitude worse than that obtained in a similar campaign with VLBA. Several factors contributed to an increase in the uncertainties in the source positions. First, the unfavourable frequency set-up resulted in an increase in the group delay uncertainties by a factor of 2.4. Retrospectively, I admit that more efforts should have been made to resolve the logistical issues with the LO frequency changes. Secondly, the size of the EVN used in this experiment is a factor of 3 smaller than the size of the VLBA network. Thirdly, the sources in the EGaPS campaign are a factor of 3 weaker than those in the VGaPS campaign.

The detection rate, 30 per cent, is significantly lower than that obtained in other survey experiments. For a comparison, the detection rate obtained in the VGaPS experiment was 76 per cent for sources in the Galactic plane pre-selected with VERA observations, and it was 36 per cent for sources selected on the basis of their spectral index. Apparently, the efficiency of the selection of the sources based on spectral index is of a level of 30–40 per cent in the Galactic plane. About 1/3 of the detected sources have a correlated flux density below 40 mJy, which makes their use as phase calibrators problematic. This indicates that the source selection strategy should be revised if a similar survey is carried out in the future.

ACKNOWLEDGMENTS

It is my pleasure to thank Yury Kovalev, David Graham, Richard Porcas, and Cormac Reynolds for useful suggestions that contributed to the success of the experiment. I would like to thank Alessandra Bertarini and Helge Rottmann for prompt recorrelation of scans with masers. I would like to thank Alan Fey for making publicly available not only the contour plots of images from the *K*/*Q* survey, but also the brightness distribution and calibrated flux densities in the FITS-format. The availability of this information was crucial for this project.

I made use of the data base CATS of the Special Astrophysical Observatory. I used in our work the data set MAI6NPANA provided by the NASA/Global Modelling and Assimilation Office (GMAO) in the framework of the MERRA atmospheric re-analysis project. The European VLBI Network is a joint facility of European, Chinese, South African, Russian and other radio-astronomy institutes funded by their national research councils. This publication makes use of data products from the Wide-field Infrared Survey Explorer, which is a joint project of the University of California, Los Angeles, and the Jet Propulsion Laboratory/California Institute of Technology, funded by NASA.

REFERENCES

Altamimi Z., Sillard P., Boucher C., 2002, J. Geopys. Res., 107, 2214
Beasley A. J., Gordon D., Peck A. B., Petrov L., MacMillan D. S., Fomalont E. B., Ma C., 2002, ApJS, 141, 13
Bourda G., Charlot P., Le Campion J.-F., 2008, A&A, 490, 403
Bourda G., Collioud A., Charlot P., Porcas R. W., Garrington S. T., 2011, A&A, 526, A102
Brunthaler A., et al., 2011, Astron. Nachr., 332, 461
Charlot P. et al., 2002, in Proc. 6th European VLBI Network Symposium, 9 http://www.mpifr-bonn.mpg.de/div/vlbi/evn2002/ book/PCharlot.pdf
Cohen M. H., Shaffer D. B., 1971, AJ, 76, 91
Condon J. J., Cotton W. D., Greisen E. W., Yin Q. F., Perley R. A., Taylor G. B., Broderick J. J., 1998, AJ, 115, 1693
Curiel S. et al., 2002, ApJ, 564, L35
Deller A. T., Tingay S. J., Bailes M., West C., 2007, PASP, 119, 318
DeMets C., Gordon R., Argus D., Stein S., 1994, Geophys. Res. Lett. 21, 2191
Fomalont E., Petrov L., McMillan D. S., Gordon D., Ma C., 2003, AJ, 126, 2562
Gregory P. C., Scott W. K., Douglas K., Condon J. J., 1996, ApJS, 103, 427
Greisen E. W., 2009, AIPS Memo, 114
Healey S. E., Romani R. W., Taylor G. B., Sadler E. M., Ricci R., Murphy T., Ulvestad J. S., Winn J. N., 2007, ApJS, 171, 61
Helmboldt J. F. et al., 2007, ApJ, 658, 203
Honma M., Kawaguchi N., Sasao T., 2000, in Buthcer H. R., ed., Proc. SPIE 4015, Radio Telescope, p. 624
Immer K. et al., 2011, ApJS, 194, 25
Kovalev Y. Y., Petrov L., Fomalont E., Gordon D., 2007, AJ, 133, 1236
Lanyi G. E. et al., 2010, AJ, 139, 1695
Ma C. et al., 1998, AJ, 116, 516
Moscadelli L., Reid M. J., Menten K. M., Brunthaler A., Zheng X. W., Xu Y., 2009, ApJ, 693, 406
Murphy T. et al., 2010, MNRAS, 420, 2403
Myers S. T. et al., 2003, MNRAS, 341, 1
Petrov L., 2011, AJ, 142, 105
Petrov L., Taylor G., 2011e, AJ, 142, 89
Petrov L., Kovalev Y. Y., Fomalont E., Gordon D., 2005, AJ, 129, 1163
Petrov L., Kovalev Y. Y., Fomalont E., Gordon D., 2006, AJ, 131, 1872
Petrov L., Kovalev Y. Y., Fomalont E., Gordon D., 2007a, AJ, 136, 580
Petrov L., Hirota T., Honma M., Shibata S. M., Jike T., Kobayashi H., 2007b, AJ, 133, 2487
Petrov L., Gordon D., Gipson J., MacMillan D., Ma C., Fomalont E., Walker R. C., Carabajal C., 2009, J. Geodesy, 83, 859
Petrov L., Honma M., Shibata S. M., 2011a, preprint (astro-ph/1107.2463)
Petrov L., Kovalev Y. Y., Fomalont E., Gordon D., 2011b, AJ, 142, 35
Petrov L., Phillips C., Bertarini A., Murphy T., Sadler E. M., 2011c, MNRAS, 414, 2528
Schaer, 1998, PhD thesis, Univ. Bern
Sunada K., Nakazato T., Ikeda N., Hongo S., Kitamura Y., Yang J., 2007, PASJ, 29, 1185

Verkhodanov O. V., Trushkin S. A., Andernach H., Chernenkov V. N., 1997, in Hunt G., Payne H. E., eds., ASP Conf. Ser. Vol. 125, Astronomical Data Analysis Software and Systems VI. Astron. Soc. Pac., San Francisco, p. 322

Walker R. C., Durand S., Kutz C., Hayward R., 2008, NRAO, VLBA Sensitivity Upgrade Memos, Memo 21, http://www.vlba.nrao.edu/memos/sensi/sensimemo21.pdf

Wrobel J., 2009, NRAO eNews, 2, 6, http://www.nrao.edu/news/newsletters/enews/enews_2_11/enews_2_11.pdf

SUPPORTING INFORMATION

Additional Supporting Information may be found in the online version of this article.

Table 4. The EGaPS catalogue of source positions of 109 target sources.

Please note: Wiley-Blackwell are not responsible for the content or functionality of any supporting materials supplied by the authors. Any queries (other than missing material) should be directed to the corresponding author for the article.

This paper has been typeset from a TEX/LATEX file prepared by the author.